

---

# A KUNG FU ATHLETE BOT THAT CAN DO IT ALL DAY: HIGHLY DYNAMIC, BALANCE-CHALLENGING MOTION DATASET AND AUTONOMOUS FALL-RESILIENT TRACKING

---

Zhongxiang Lei<sup>1</sup> Lulu Cao<sup>1,2</sup> Xuyang Wang<sup>1,2</sup> Tianyi Qian<sup>4†</sup> Jinyan Liu<sup>1†</sup> Xuesong Li<sup>1†</sup>

<sup>1</sup> Beijing Institute of Technology

<sup>2</sup> Equal contribution

<sup>4</sup> QIYUAN Lab

† Corresponding authors

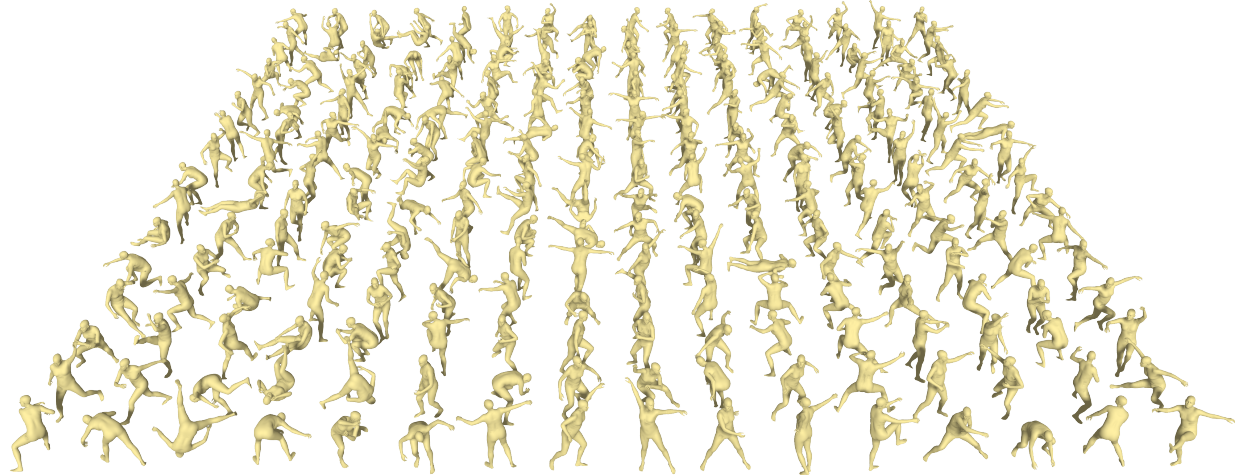


Figure 1: Teaser of the KungFuAthlete dataset. Visualization of reconstructed full-body motions from daily training videos of professional martial artists. The dataset spans a wide spectrum of motion dynamics, from non-jumping ground actions to highly dynamic acrobatic jumps, resulting in significantly larger joint velocities and body-level dynamics than existing human motion datasets. This diversity makes KungFuAthlete particularly suitable for pushing the boundaries of humanoid motion and exploring the current limits of robotic capabilities.

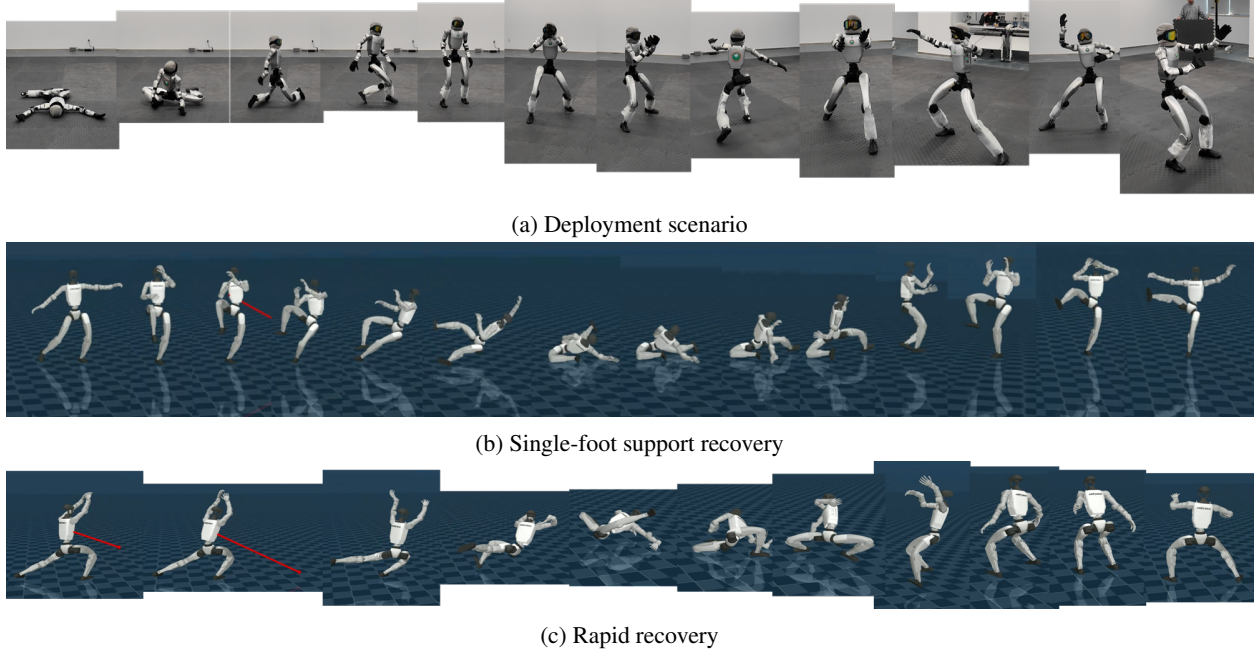


Figure 2: Overall experimental demonstration. The red arrows indicate the direction and magnitude of the pulling force on the torso, with longer lines representing greater force.

## ABSTRACT

Current humanoid motion tracking systems can execute routine and moderately dynamic behaviors, yet significant gaps remain near hardware performance limits and algorithmic robustness boundaries. Martial arts represent an extreme case of highly dynamic human motion, characterized by rapid center-of-mass shifts, complex coordination, and abrupt posture transitions. However, datasets tailored to such high-intensity scenarios remain scarce. To address this gap, we construct KungFuAthlete, a high-dynamic martial arts motion dataset derived from professional athletes' daily training videos. The dataset includes ground and jump subsets covering representative complex motion patterns. The jump subset exhibits substantially higher joint, linear, and angular velocities compared to commonly used datasets such as LAFAN1, PHUMA, and AMASS, indicating significantly increased motion intensity and complexity. Importantly, even professional athletes may fail during highly dynamic movements. Similarly, humanoid robots are prone to instability and falls under external disturbances or execution errors. Most prior work assumes motion execution remains within safe states and lacks a unified strategy for modeling unsafe states and enabling reliable autonomous recovery. We propose a novel training paradigm that enables a single policy to jointly learn high-dynamic motion tracking and fall recovery, unifying agile execution and stabilization within one framework. This framework expands robotic capability from pure motion tracking to recovery-enabled execution, promoting more robust and autonomous humanoid performance in real-world high-dynamic scenarios. We provide videos and an open-source dataset at <https://kungfuathletebot.github.io/>.

## 1 Introduction

Humanoid robots are considered a key platform for future applications in service industries, manufacturing, and other fields. Their ability to move autonomously and stably[1, 2, 3], and to recover from disturbances without human intervention[4, 5], represents a current research hotspot. However, this emerging platform still lacks sufficient data support during its initial development phase. While existing motion tracking technologies can effectively capture everyday movements[6, 7, 8, 9], the upper limits of robotic hardware performance require further exploration, making the construction of higher-dynamic datasets urgently needed. Simultaneously, high-dynamic actions carry high failure rates, necessitating research into methods that enable safe falls and autonomous recovery under a single strategy to reduce reliance on humans or auxiliary devices. This paper aims to construct a high-dynamic action dataset and, while

learning from this data, enable robots to protect themselves and recover safely, laying the foundation for robots to move beyond the laboratory and reduce human intervention.

The construction of high-dynamic motion datasets and corresponding algorithms is urgent, as it provides the foundation for future robots to maintain stability and precision in complex tasks. Existing open-source motion capture datasets primarily focus on human daily activities, such as the AMASS [10] dataset, which has been extensively studied. Recent frameworks like GMT [11], TWIST [12], and other expert systems can track complete motion sequences under a single policy. Although the LaFAN1 [13] dataset provides long-duration, high-dynamic motion data, existing research (e.g., AdaMimic [14], BeyondMimic [15]) struggles to meet the demands of adjusting robotic hardware performance limits. This paper collaborates with national-level martial arts athletes to generate a high-dynamic motion dataset from their daily training videos, aiming to extract large-scale training data. However, such data still suffers from jitter and highly unpredictable inaccuracies, for which existing research offers no effective solutions.

Unifying motion tracking and fall recovery within a single strategy holds significant importance. During high-dynamic motion execution, robots often encounter unknown disturbances or challenging maneuvers, leading to increased failure rates. Upon failure, robots may lose autonomy and suffer equipment damage, necessitating human intervention—a scenario incompatible with achieving future autonomous robotic operation goals. Although existing research has proposed methods for standing from fallen postures [16, 17, 18] and safe falling [19, 20], these approaches cannot simultaneously accomplish motion tracking and fall recovery within a single strategy, failing to meet the deployment requirements of real-world scenarios.

In summary, the main contributions of this paper include:

- **High-Dynamic Martial Arts Action Dataset** A large-scale high-dynamic action dataset has been released, featuring action sequences extracted from daily training videos of top martial artists. It contains a substantial number of actions characterized by significant center-of-gravity shifts and large dynamic amplitudes.
- **Root Node Height Drift Correction** Addressing the prevalent issue of root node height drift during video-to-motion reconstruction, a height correction algorithm is proposed.
- **End-to-End Motion Tracking Paradigm with Autonomous Fall Recovery** Proposed a training paradigm that simultaneously trains a policy for high-dynamic motion tracking and autonomous fall recovery, enabling recovery from any state back to the referenced motion without requiring reference standing-up actions.

## 2 Related Works

### 2.1 Robot Motion Tracking Data and Capture Methods

Due to the lack of large-scale motion datasets specifically designed for humanoid robots, existing research often relies on redirecting motion capture data originally used for animation and human modeling to robotic platforms. Typical examples include the AMASS dataset [10], which uniformly parameterizes multi-source optical motion capture data, and LaFAN1 [13], frequently used in motion interpolation and redirection studies. Such datasets offer distinct advantages in motion naturalness and continuity, finding widespread application in humanoid robot motion imitation and full-body control tasks. However, their content primarily focuses on low-to-medium dynamic behaviors like walking, turning, and sitting, with limited overall dynamic range and center-of-mass displacement. This restricts coverage of high-dynamic actions such as jumping, rapid turning, or abrupt posture transitions, thereby failing to effectively challenge the performance limits of robotic hardware. Although recent work has fully exploited the potential of AMASS and LaFAN1, achieving stable and high-quality humanoid control within their coverage, a general-purpose action dataset featuring high dynamics, long sequences, and significant center-of-mass transformations remains lacking. Some studies have attempted to collect higher-quality data through hardware-based approaches, such as HOMIE [21] and HumanoidExo [22] using exoskeletons or wearable devices, as well as VR-based MoCap-free acquisition systems like TWIST2 [23] and SONIC [24]. These methods yield physically consistent, high-fidelity motion data but rely on specialized hardware, resulting in high acquisition costs and limited scalability.

In recent years, research has shifted toward constructing motion data from real-world videos to address the scarcity of high-dynamic motion data. Monocular video-based human motion reconstruction methods, such as GVHMR [25] and PromptHMR [25], can recover complex task motions from large-scale internet videos, significantly expanding the diversity and dynamic range of the action distribution. Compared to hardware motion capture, video data offers distinct advantages in acquisition cost, scale, and scenario coverage, making it an attractive avenue for constructing high-dynamic motion datasets. However, constrained by visual reconstruction accuracy and temporal consistency, motion sequences generated by these methods commonly suffer from global pose drift, temporal jitter, and error accumulation—problems exacerbated in long sequences or high-dynamic scenarios—rendering them unsuitable for

direct application in high-precision humanoid robot control. Nevertheless, the characteristics of video data—large scale, low cost, but noisy quality—make it an indispensable data source in current high-dynamic humanoid motion learning, highlighting the urgent need for noise-robust learning and control methods.

## 2.2 High-Dynamic Motion Tracking

Due to the lack of more challenging actions in the AMASS and LAFAN1 datasets, recent studies often construct custom datasets when handling highly dynamic actions. For instance, ASAP [26] and KungfuBot [27] utilize monocular video-based human motion reconstruction methods to redirect self-recorded human action videos into robotic motions, thereby generating more expressive and flexible datasets. Although ASAP designed strategies like symmetric Actor-Critic (AC) training and interference-terminated curricula for this dataset, errors inherent in the dataset necessitated precise alignment of high-dynamic actions through the Delta Action Model and fine-tuning. KungfuBot, grounded in physical principles such as center-of-mass calculations, filters the dataset and combines curricula with domain randomization to achieve high-dynamic human behavior tracking.

HuB [28] and Agility Meets Stability [29] focus on foot and center-of-mass processing to address data drift. HuB corrects data by reading foot positions during single-leg actions, filters data using center-of-mass calculations, and designs center-of-mass-related rewards to maintain stability. Agility Meets Stability optimizes the distance between the center of mass and the supporting foot to align the dataset with physical laws, combining adaptive rewards and learning strategies to achieve stability in high-dynamic motion tracking.

To enhance the expressiveness and dynamism of motion tracking, Exbody2[30] filters motion data and defines independent policies for fine-tuning different high-dynamic actions; Adamimic [14] employs keyframe selection to divide motion tracking into two stages: fixed-interval motion tracking and adaptive-interval Adapters Learning, enabling high-difficulty motion tracking. However, it heavily relies on the quality of manually selected keyframes and struggles to sustain high-dynamic tracking over extended periods.

Robot Dancing [31] achieves long-duration high-dynamic motion tracking through residual networks and domain randomization; BeyondMimic [15] employs diffusion models, unique sampling techniques, and residual modules to track prolonged high-dynamic actions, yet stability remains challenging. However, it may still experience falls during certain complex actions, and once a fall occurs, subsequent actions cannot be completed.

## 2.3 Recovery

In recent years, reinforcement learning (RL) has been increasingly applied to post-fall recovery for humanoid robots. For instance, HumanUP [32] and HoST [33] achieved stable standing recovery across diverse initial fall poses and environments without requiring additional training data. Unified Humanoid Get-Up [34] further introduced a unified RL strategy enabling “zero-shot” recovery for humanoid robots of varying morphologies after falls. However, these studies treat post-fall recovery as an isolated task, focusing exclusively on posture reset once the robot has already fallen. To address this limitation, SafeFall [19] proposed a dual-policy RL framework that integrates task execution with fall protection, automatically switching to a protective mode during unexpected falls to mitigate impact. FIRM [17] extended this idea by learning an integrated policy from limited demonstration data, unifying fall prevention, impact mitigation, and post-fall recovery into a single end-to-end strategy. This approach enables autonomous handling of the entire fall process—from risk prediction and impact buffering to post-fall recovery—overcoming the delays and coordination issues inherent in segmented policies. BFM-Zero [18] achieves the integration of motion tracking and fall recovery tasks within a unified policy framework. However, its core algorithm is not based on a pure reinforcement learning paradigm, and the acquisition of fall recovery capabilities still relies on auxiliary guidance from a small amount of data. In quadruped robotics, CHRL [16] proposed an RL framework tailored for high-dynamic scenarios, allowing quadrupeds to recover from unexpected falls during rapid locomotion and turning maneuvers.

# 3 Kongfu Athletes Dataset : Conversion and Correction of High-Dynamic-Range Video

## 3.1 Data Overview

The data originates from athletes’ daily training videos, totaling 197 clips. Each dataset may consist of multiple merged segments. We employed automatic segmentation to divide the videos into 1,726 sub-segments, ensuring most videos lacked abrupt transitions that could cause excessive variations in motion capture data. These sub-clips were processed using GVHMR, followed by GMR for reorientation. The processed dataset primarily consists of routine training videos, totaling 848 samples. Among these, 715 samples (approximately 84%) do not represent distinct martial arts techniques, mainly reflecting standard training processes and practice scenarios. Among specialized movements,

Category	Count	Example Subcategories
Daily Training	715	—
Fist	53	Long Fist (33), Tai Chi Fist (14), Southern Fist (6)
Staff	30	Staff Technique (30)
Skills	28	Backflip (12), Lotus Swing (9)
Saber	15	Southern Saber (15), Tai Chi Sword (7)

boxing techniques accounted for the highest proportion (53 samples), dominated internally by Changquan (33 samples) while also covering Taijiquan (14 samples) and Southern boxing (6 samples), highlighting boxing’s central role in training and demonstrations. Staff techniques comprised 30 samples, all focused on standardized staff movements. Skill-based techniques comprised 28 samples, primarily consisting of jumps and flips such as somersaults and lotus swings, indicating a concentrated distribution of high-difficulty physical skills. Among weapon techniques, knife forms were represented by Southern-style knives (15), while sword forms were exclusively Tai Chi swords (7).

Table 1: Statistical comparison of motion datasets. All reported metrics are averaged over the entire dataset.

Dataset	FPS	Joint Vel.	Body Lin. Vel.	Body Ang. Vel.	Frames
LAFAN1	50.0	0.00142	0.00021	0.01147	10749.23
PHUMA	50.0	0.00120	0.00440	-0.00131	169.59
AMASS	30.0	0.00048	-0.00568	0.00903	370.65
KungFuAthlete (Ground)	50.0	-0.00199	0.01057	0.04034	577.68
KungFuAthlete (Jump)	50.0	0.02384	0.05297	0.18017	397.21

As shown in Table 1, we categorized the dataset based on the presence or absence of jumping movements: KungFuAthlete (Ground) contains non-jumping actions, while KungFuAthlete (Jump) includes jumping actions. Comprehensive category distribution statistics and kinematic metrics reveal that the KungFuAthlete dataset distinctly differs from general human motion datasets in terms of movement intensity and action complexity. In terms of overall category composition, this dataset centers on daily training supplemented by boxing techniques, weaponry, and acrobatic maneuvers. Notably, the acrobatic category concentrates high-dynamic jumping actions like somersaults and cartwheels. This structure directly manifests in statistical characteristics: the Jump subset exhibits significantly higher joint velocity, body linear velocity, and angular velocity than other datasets (joint vel, body lin vel w, and body ang vel all reach the highest levels among comparable datasets). In contrast, the Ground subset excludes jumping movements. While its velocity and angular velocity metrics remain higher than those of daily/natural motion datasets like LAFAN1 and AMASS, they are notably lower than the Jump subset. This reflects the martial arts training characteristics centered on continuous ground-based power generation, rapid body rotations, and weapon manipulation. Compared to datasets like PHUMA and AMASS, which focus on natural walking or daily activities, KungFuAthlete exhibits greater dynamic amplitude and stronger non-stationarity at the same or higher frame rates. This indicates that it not only contains more intense body movements but also covers more challenging transient motion patterns.

### 3.2 Root Node Height Drift and Local Jitter Correction

Data extracted from video footage presents the following issues: 1. Height positioning inaccuracies occur when subjects jump or exhibit excessive leg movements, as shown in Figure 3 where the subject appears suspended in mid-air. Since the robot’s height is calculated relative to the root node, the algorithm primarily focuses on correcting the root node. 2. As shown in Figure 2 (not implemented), since the algorithm captures single-frame s and then stitches them into a video, the connected local frames become discontinuous, causing local jitter. This section proposes a method to address both issues.

#### 3.2.1 Root Node Height Drift Method

Given a retargeted pose sequence

$$\mathcal{Q} = \{\mathbf{q}_t\}_{t=1}^T, \quad \mathbf{q}_t = [\mathbf{p}_t, \mathbf{r}_t, \boldsymbol{\theta}_t], \quad (1)$$

we focus on correcting the temporal trajectory of the root height

$$P(t) = p_t^{(z)}, \quad (2)$$

where  $p_t^{(z)}$  denotes the vertical component of the root position.

---

**Algorithm 1** Root Height Drift Correction with Parabolic Jump Reconstruction

---

**Require:** Retargeted pose sequence  $Q = \{\mathbf{q}_t\}_{t=1}^T$ , gravity constant  $g$ , velocity threshold  $\tau$   
**Ensure:** Corrected pose sequence  $\hat{Q}$

```

1: Extract root height trajectory  $P(t) = p_t^{(z)}$ 
2: Compute forward root velocity  $\dot{P}(t) = P(t+1) - P(t)$ 
3: Detect local maxima  $\mathcal{M}_{\max}$  and local minima  $\mathcal{M}_{\min}$  of  $P(t)$ 
4: Initialize reconstructed trajectory  $\hat{P}(1) \leftarrow P(1) - z_{\min}(\mathbf{q}_1)$ 
5: for  $t = 2$  to  $T$  do
6:   if  $t \in \mathcal{M}_{\min}$  then
7:      $\tilde{P} \leftarrow P(t) - z_{\min}(\mathbf{q}_t)$ 
8:     if  $z_{\min}(\tilde{\mathbf{q}}_t) \geq 0$  then
9:        $\hat{P}(t) \leftarrow \tilde{P}$ 
10:      continue
11:     end if
12:   end if
13:    $\hat{P}(t) \leftarrow \hat{P}(t-1) + \mathbb{I}[\dot{P}(t-1) > \tau] \cdot \dot{P}(t-1)$ 
14: end for
15: for each  $t_s \in \mathcal{M}_{\max}$  do
16:   Find the nearest  $t_e > t_s$  such that  $t_e \in \mathcal{M}_{\min}$ 
17:    $N \leftarrow t_e - t_s - 1$ 
18:   Solve  $T = \sqrt{\frac{2(\hat{P}(t_s) - \hat{P}(t_e))}{g}}$ 
19:   for  $k = 1$  to  $N$  do
20:      $\Delta t_k \leftarrow \frac{k}{N+1}T$ 
21:      $\hat{P}(t_s + k) \leftarrow \hat{P}(t_s) - \frac{1}{2}g\Delta t_k^2$ 
22:   end for
23: end for
24: for  $t = 1$  to  $T$  do
25:   if  $z_{\min}(\tilde{\mathbf{q}}_t) < 0$  then
26:      $\hat{P}(t) \leftarrow P(t) - z_{\min}(\mathbf{q}_t)$ 
27:   end if
28: end for
29: Update  $\hat{q}_t^{(z)} \leftarrow \hat{P}(t)$  for all  $t$ 
30: return  $\hat{Q}$ 

```

---

In practice, retargeted motions often suffer from *root height drift*, leading to physically implausible floating artifacts or ground penetration, especially in non-jumping motions. To address this issue, we propose a *piecewise root height reconstruction strategy* that enforces ground contact consistency while preserving the original motion dynamics.

### 3.2.2 Minimum Body Height Constraint

Let  $z_i(\mathbf{q}_t)$  denote the height of the  $i$ -th body part at time  $t$ . The minimum body height is defined as

$$z_{\min}(\mathbf{q}_t) = \min_{i \in \mathcal{B}} z_i(\mathbf{q}_t), \quad (3)$$

where  $\mathcal{B}$  denotes the set of all robot body parts.

For frames corresponding to *ground-contact phases*, the physically valid root height is obtained by aligning the lowest body part with the ground plane:

$$\hat{p}_t^{(z)} = p_t^{(z)} - z_{\min}(\mathbf{q}_t). \quad (4)$$

This operation enforces the ground-contact constraint

$$z_{\min}(\hat{\mathbf{q}}_t) \begin{cases} = 0, & \text{for non-jumping (contact) phases,} \\ \geq 0, & \text{for jumping (airborne) phases,} \end{cases} \quad (5)$$

ensuring exact ground contact during support phases while allowing positive clearance during airborne motion.

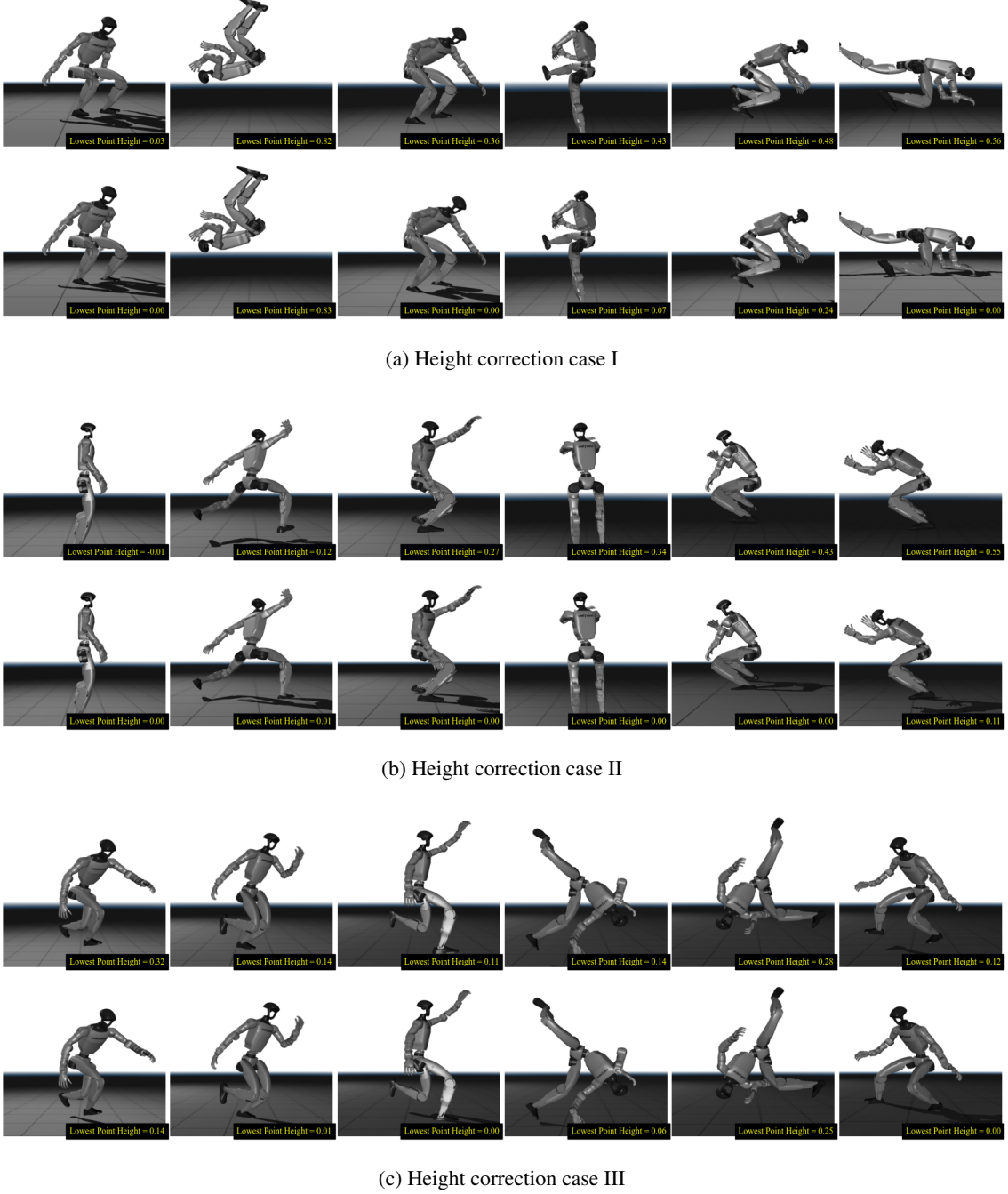


Figure 3: Illustration of the height data correction process.

### 3.2.3 Temporal Propagation with Velocity Thresholding

To avoid introducing temporal discontinuities, the root height is not overwritten at every timestep. Instead, we estimate the root vertical velocity using a first-order forward difference:

$$\dot{P}(t) = P(t+1) - P(t). \quad (6)$$

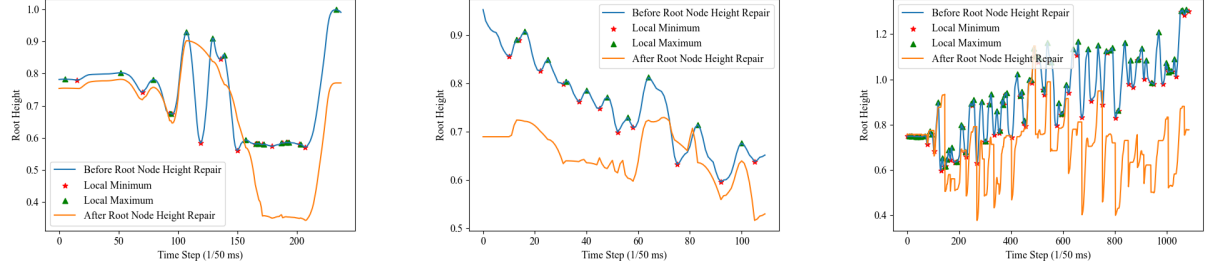


Figure 4: Corrected Root Node Curve Diagram.

For frames that are not detected as reliable ground-contact points, the corrected root height is propagated from the previous timestep:

$$\hat{P}(t) = \hat{P}(t-1) + \begin{cases} \dot{\hat{P}}(t-1), & \text{if } \dot{\hat{P}}(t-1) > \tau, \\ 0, & \text{otherwise,} \end{cases} \quad (7)$$

where  $\tau$  is a small velocity threshold used to suppress spurious vertical jitter.

This design follows the implementation logic in the code and ensures temporal smoothness while preventing unrealistic upward drift.

### 3.2.4 Jump Phase Handling via Local Extrema

Jumping motions require special treatment, as enforcing continuous ground contact would destroy the ballistic structure of the motion. We therefore analyze the root height trajectory  $P(t)$  and detect local extrema:

- **Local maxima:**  $P'(t) = 0, P''(t) < 0$  (take-off apex),
- **Local minima:**  $P'(t) = 0, P''(t) > 0$  (landing contact).

For each detected jump segment bounded by a local maximum  $t_{\max}$  and a subsequent local minimum  $t_{\min}$ , we reconstruct the intermediate root heights using a parabolic interpolation:

$$\hat{P}(t) = \text{Parabola}(\hat{P}(t_{\max}), \hat{P}(t_{\min})), \quad t \in (t_{\max}, t_{\min}), \quad (8)$$

which preserves the smooth airborne trajectory observed in natural jumping motions.

Certain extrema corresponding to non-jumping behaviors (e.g., squatting or standing up) are excluded via a manually defined skip set, consistent with the implementation.

### 3.2.5 Parabolic Reconstruction of Airborne Root Motion

For jump phases, enforcing continuous ground contact would destroy the ballistic structure of the motion. Therefore, for each airborne segment bounded by a take-off frame  $t_s$  and a landing frame  $t_e$ , we explicitly reconstruct the root height trajectory using a physics-inspired parabolic model.

Let the corrected root heights at the segment boundaries be

$$\hat{P}(t_s) = y_0, \quad \hat{P}(t_e) = y_1, \quad (9)$$

with  $y_0 > y_1$ . We assume that the vertical motion during the airborne phase follows constant gravitational acceleration and zero initial vertical velocity at take-off. Under this assumption, the vertical trajectory is modeled as

$$y(t) = y_0 - \frac{1}{2}gt^2, \quad (10)$$

where  $g$  denotes the gravitational acceleration constant.

The terminal time  $T$  is determined by enforcing the landing height constraint:

$$y(T) = y_1 \quad \Rightarrow \quad T = \sqrt{\frac{2(y_0 - y_1)}{g}}. \quad (11)$$

We then uniformly sample  $N$  intermediate time instants within the open interval  $(0, T)$ , yielding a set of reconstructed root heights

$$\left\{ \hat{P}(t_s + \Delta t_k) \right\}_{k=1}^N, \quad \Delta t_k = \frac{k}{N+1} T. \quad (12)$$

These samples replace the root height values between  $t_s$  and  $t_e$ , ensuring a smooth and physically plausible airborne trajectory.

### 3.2.6 Final Ground Penetration Correction

As a final safeguard, we enforce the ground constraint for all frames:

$$\text{if } z_{\min}(\hat{\mathbf{q}}_t) < 0, \quad \hat{p}_t^{(z)} = p_t^{(z)} - z_{\min}(\mathbf{q}_t). \quad (13)$$

This guarantees strict non-penetration of the ground across the entire sequence.

## 3.3 Post-Processing via Savitzky–Golay Smoothing

Since the algorithm captures single-frame poses and then stitches them into video, this results in discontinuities between connected local frames, causing localized jitter. To further improve temporal smoothness while preserving the overall motion structure, we apply a **Savitzky–Golay [35](SG) filter** to the corrected pose sequence.

Formally, given the corrected trajectory

$$\hat{\mathbf{q}}_t = [\hat{\mathbf{p}}_t, \hat{\mathbf{r}}_t, \hat{\boldsymbol{\theta}}_t], \quad t = 1, \dots, T,$$

we independently filter each component of the root position and joint angles:

$$\tilde{\mathbf{q}}_t^{(i)} = \text{SG}(\{\mathbf{q}_k^{(i)}\}_{k=1}^T), \quad i = 1, \dots, N,$$

where  $\text{SG}(\cdot)$  denotes the Savitzky–Golay smoothing operator with polynomial order  $p$  and window length  $w$ . The window length is chosen adaptively based on the sequence length, with a default of approximately 1/10 of the total frames, while ensuring an odd number of samples for symmetric fitting.

This procedure preserves **local extrema and motion peaks**, which are crucial for jump apexes and contact phases, while removing small jitters. Empirically, it produces visually smoother and physically plausible trajectories, particularly beneficial for downstream motion retargeting or control tasks.

## 4 End-to-End Motion Tracking with Autonomous Fall Recovery

### 4.1 Objective

The ability to autonomously recover from high-dynamic motions is a critical capability for robotic systems, as it enables greater autonomy, reduces reliance on human intervention, and alleviates the need for safety cages. We formulate autonomous fall recovery motion tracking as a task of recovering from arbitrary initial states to a desired target state, and define an end-to-end (one policy) reward objective for this task as follows:

$$\max_{\pi} \mathbb{E}_{\pi} \left[ \sum_{k=0}^{\infty} \gamma^k \left( r_{\text{mt}} + \mathbb{I}_{\text{rc}}(k) r_{\text{rc}} \right) \middle| \begin{array}{l} z \sim \text{Bernoulli}(p), \\ \mathbf{q}_0 = \begin{cases} \mathbf{q}_0^{\text{ref}}, & z = 1, \\ \sim \mathcal{D}_{\text{GRSI}}, & z = 0, \end{cases} \\ \mathbf{q}_{0:\infty}^{\text{ref}} = (\mathbf{q}_0^{\text{ref}}, \mathbf{q}_1^{\text{ref}}, \dots) \sim \text{low kinetic energy sampling (sec. 4.2) from } \mathcal{D}_{\text{ref}} \end{array} \right], \quad (14)$$

where

- $p$  is the probability of executing motion tracking, and  $1 - p$  is the probability of executing fall recovery.
- $\mathbf{q}_k$  denotes the robot state at timestep  $k$ .
- $\mathbf{q}_k^{\text{ref}}$  denotes the reference motion state at timestep  $k$ .
- $r_{\text{mt}}$  is the physics-based *motion tracking reward*, and  $r_{\text{rc}}$  is the *recovery reward*, both formulated as reference-conditioned functions of  $\mathbf{q}_k$  and  $\mathbf{q}_k^{\text{ref}}$ .

- $\mathbb{I}_{rc}(k)$  is the recovery indicator function, defined as

$$\mathbb{I}_{rc}(k) = \mathbb{I}(|h_{\text{ref}}(\mathbf{q}_k^{\text{ref}}) - h_{\text{robot}}(\mathbf{q}_k)| > \tau),$$

where  $h_{\text{ref}}(\mathbf{q}_k^{\text{ref}})$  and  $h_{\text{robot}}(\mathbf{q}_k)$  denote the shoulder height of the reference motion and the robot at timestep  $k$ , respectively, and  $\tau$  is a threshold.

- $\mathcal{D}_{\text{ref}}$  is the reference motion dataset.
- $\mathcal{D}_{\text{GRSI}}$  is the dataset of gravity-based fall poses introduced in Section 4.5.

To learn the objective Eq. 14, we employ FastSAC [36, 37] for policy learning. FastSAC is an off-policy reinforcement learning method based on the maximum entropy principle. It maintains a random policy and two Q-functions, achieving efficient data reuse through experience replay. During training, the algorithm samples mini-batches of transition data from the replay pool. It constructs target Q-values incorporating an entropy regularization term using the current policy to sample actions in the next state, then updates both critics by simultaneously minimizing Bellman errors. Unlike dual-Q structures using minimums, FastSAC averages outputs from both critics to mitigate overly conservative value estimates in large-scale parallel training and high-dimensional continuous control scenarios. The policy network updates via reparameterization tricks, explicitly encouraging policy entropy to boost exploration efficiency while maximizing expected return; entropy temperature parameters adaptively adjust through target entropy constraints. These updates are executed multiple times after each environmental interaction, fully leveraging parallel simulation data to significantly accelerate convergence while ensuring training stability.

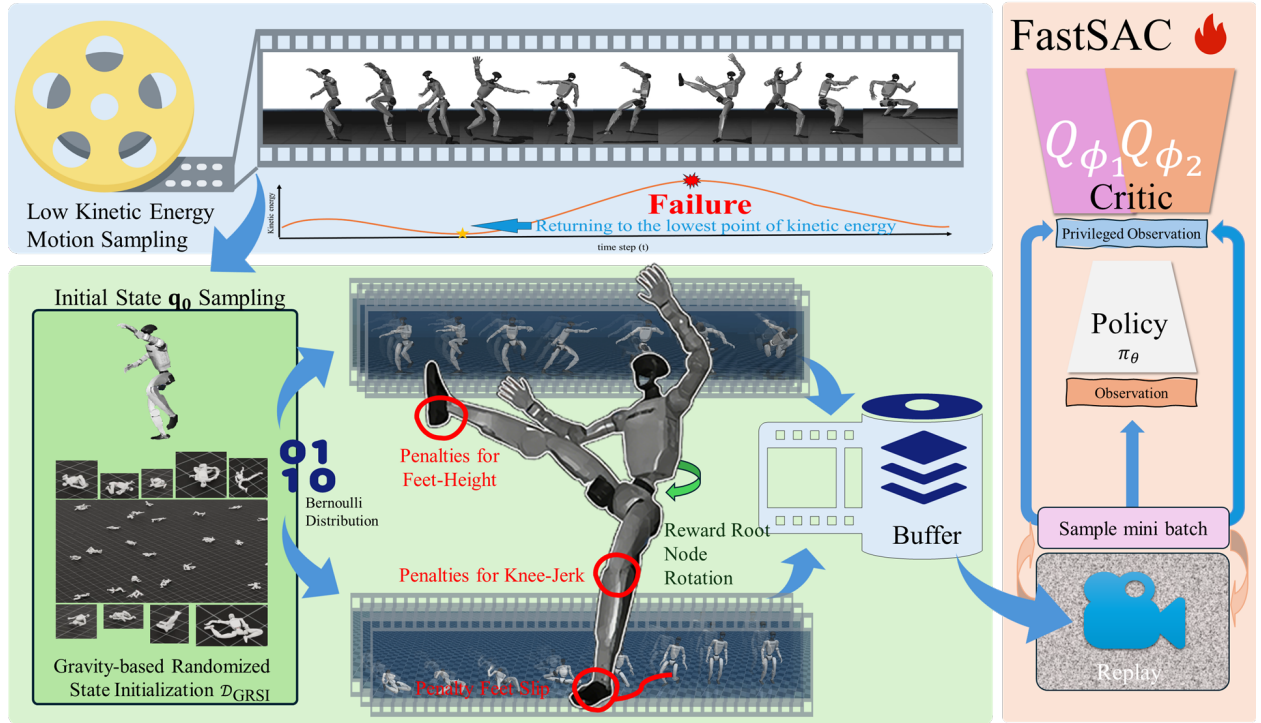


Figure 5: Flowchart of training a policy using FastSAC for high-dynamic tracking and autonomous fall recovery without reference frames under low-kinetic-energy sampling.

## 4.2 Low Kinetic Energy Sampling

BeyondMimic employs a failure-driven adaptive timestep sampling strategy by increasing the sampling probability of motion segments with high failure frequency. However, in highly dynamic motions, failures often occur at aerial or high-kinetic-energy phases, where the robot state is physically unrecoverable within a single episode, leading to a failure feedback loop.

Let the reference motion dataset be denoted as  $\mathcal{D}_{\text{ref}} = \{\mathbf{q}_{0:T}^{\text{ref}}, \dot{\mathbf{q}}_{0:T}^{\text{ref}}\}$ , where  $\mathbf{q}_t^{\text{ref}} \in \mathbb{R}^{|\mathcal{J}|}$  and  $\dot{\mathbf{q}}_t^{\text{ref}} \in \mathbb{R}^{|\mathcal{J}|}$  represent the reference joint positions and joint velocities at timestep  $t$ , and  $\mathcal{J}$  denotes the set of robot joints.

To avoid initializing episodes from dynamically unrecoverable states, we define a scalar kinetic-energy proxy for each reference timestep as

$$E(t) = \sum_{j \in \mathcal{J}} |\dot{q}_{t,j}^{\text{ref}}|, \quad (15)$$

where  $\dot{q}_{t,j}^{\text{ref}}$  denotes the velocity of joint  $j$  at timestep  $t$ .

We identify a set of low-kinetic-energy anchor timesteps  $\mathcal{B} = \{b_1, b_2, \dots, b_K\} \subset \{0, \dots, T\}$ , corresponding to local minima of  $E(t)$  along the reference trajectory. Episode initial states are restricted to be sampled from these anchors.

Each anchor timestep  $b_k \in \mathcal{B}$  is associated with a non-negative sampling weight  $w_k$ , which is initialized to  $w_k = 1$  for all  $k$ . When an episode terminates at reference timestep  $t_f$ , the failure is attributed to the nearest preceding anchor

$$k^* = \arg \max_k \{b_k \mid b_k \leq t_f\}, \quad (16)$$

and the corresponding weight is updated according to

$$w_{k^*} \leftarrow \text{clip}(w_{k^*} + \alpha, w_{\min}, w_{\max}), \quad (17)$$

while all other weights remain unchanged.

Finally, reference initial states are sampled according to the categorical distribution

$$p(b_k) = \frac{w_k}{\sum_{k'=1}^K w_{k'}}, \quad (18)$$

and the corresponding reference trajectory  $\mathbf{q}_{0:\infty}^{\text{ref}} = (\mathbf{q}_{b_k}^{\text{ref}}, \mathbf{q}_{b_k+1}^{\text{ref}}, \dots)$  is used to initialize the episode.

### 4.3 Reward Design

#### 4.3.1 Physics Stability Reward $r_{mt}$ Design for High-Speed Motion

Table 2: Physics stability motion tracking reward  $r_{mt}$

Name	Expression	Weight
Motion Relative Body Position Error [15]	$\exp\left(-\frac{1}{\sigma^2} \frac{1}{B} \sum_b \ \mathbf{p}_b^{\text{rel}} - \hat{\mathbf{p}}_b\ ^2\right)$	4.0
Motion Relative Body Orientation Error [15]	$\exp\left(-\frac{1}{\sigma^2} \frac{1}{B} \sum_b \ \text{quat\_error}(\mathbf{q}_b^{\text{rel}}, \hat{\mathbf{q}}_b)\ ^2\right)$	2.0
Motion Global Body Angular Velocity [15]	$\exp\left(-\frac{1}{\sigma^2} \frac{1}{B} \sum_b \ \boldsymbol{\omega}_b - \hat{\boldsymbol{\omega}}_b\ ^2\right)$	1.0
Motion Center of Mass [28]	$\exp\left(-\frac{\ \mathbf{c}_{xy} - \mathbf{f}_{\text{min},xy}\ }{\sigma_{\text{COM}}^2}\right) \cdot \mathbf{1}_{\text{unbalanced}}$	2.0
Motion Close Feet [28]	$\max(0, 0.16 - \ \mathbf{f}_{\text{left}} - \mathbf{f}_{\text{right}}\ )$	-1000
Feet Slip [38]	$\sum_f \sqrt{\ \mathbf{v}_f^{xy}\ } \cdot \mathbf{1}_{\text{contact}_f > \text{threshold}}$	-2.0
Penalty Relative Root Orientation	$\sum_b \ \text{quat\_error}(\mathbf{q}_{\text{root}}^{\text{rel}}, \hat{\mathbf{q}}_{\text{root}})\ ^2$	-1.0
Penalty Action Rate (Knee)	$\sum_{j \in \text{knee}} \ a_j - a_j^{\text{prev}}\ ^2$	-3
Penalty Action Rate (Ankle)	$\sum_{j \in \text{ankle}} \ a_j - a_j^{\text{prev}}\ ^2$	-20
Limits DOF Position [37]	$\sum_j [(\text{clip}(p_j - \text{upper}_j, 0, \infty)) + (\text{clip}(\text{lower}_j - p_j, 0, \infty))]$	-100
Undesired contacts [15, 37]	$\sum_{i \in \mathcal{B}_{\text{undesired}}} \mathbb{I}(F_i > \gamma)$	-0.5

To ensure physically plausible and dynamically stable humanoid motions, we have organized a set of reward and penalty terms (Table. 2 for whole-body control. The *Motion Relative Body Position Error*, *Motion Relative Body*

*Orientation Error*, and *Motion Global Body Angular Velocity* encourage the robot to closely track the reference motion in position, orientation, and angular velocity, where  $B$  denotes the number of tracked body parts,  $\mathbf{p}_b^{\text{rel}}$  and  $\mathbf{q}_b^{\text{rel}}$  are the relative positions and quaternions, and  $\hat{\mathbf{p}}_b$  and  $\hat{\mathbf{q}}_b$  represent the robot's actual states. The *Center-of-Mass Error* and *Feet Proximity* terms guide the robot to maintain balance, where  $\mathbf{c}_{xy}$  is the XY-plane position of the center of mass,  $\mathbf{f}_{\min, xy}$  is the XY-plane position of the lowest foot, and  $\mathbf{1}_{\text{unbalanced}}$  is an indicator of whether the robot has fallen, by aligning the center of mass with the supporting foot and keeping the feet sufficiently close.

For high-dynamics tasks, we have organized task-specific penalties to enhance stability. The *Relative Root Orientation Penalty* is used in high-speed turning tasks to ensure the robot can track rapid body rotations. The *Feet Slip Penalty* is applied in center-of-mass transition tasks, penalizing foot dragging and encouraging the robot to lift the non-supporting foot during weight shifts. The *Knee and Ankle Action Rate Penalties* prevent excessive actuation of the knee and ankle joints during weight transfer, reducing oscillations and promoting smooth motion. The *Soft DOF Limit Penalty* constrains joint positions via clipping to prevent exceeding soft limits, ensuring feasibility. Overall, these reward and penalty terms balance motion tracking fidelity with physical plausibility.

#### 4.3.2 Autonomous Fall Recovery Reward $r_{\text{rc}}$ Design

Table 3: Fall Recovery Reward  $r_{\text{rc}}$

Name	Expression	Weight
Penalty Relative Shoulder Height	$\sum_{b \in \text{shoulder}} \ (\mathbf{p}_b^{\text{rel}})_z - (\hat{\mathbf{p}}_b)_z\ ^2$	-2.0
Penalty XY Root Movement Before Stand	$\mathbf{1}_{\ (\mathbf{p}_{\text{shoulder}}^{\text{rel}})_z - (\hat{\mathbf{p}}_{\text{shoulder}})_z\  > \epsilon} \cdot \ \mathbf{c}_{xy} - \mathbf{c}_{xy}^{\text{prev}}\ $	-1.0
Penalty Action Rate Before Stand	$\mathbf{1}_{\ (\mathbf{p}_{\text{shoulder}}^{\text{rel}})_z - (\hat{\mathbf{p}}_{\text{shoulder}})_z\  > \epsilon} \cdot \sum_j \ a_j - a_j^{\text{prev}}\ ^2$	-2.0

Recovering rewards (Table. 3) are designed to promote stable standing from arbitrary initial configurations. The Penalty XY Root Movement Before Stand term ( $\mathbf{c}_{xy}$ ) penalizes horizontal translation of the robot root when the shoulder height ( $\mathbf{p}_{\text{shoulder}}^{\text{rel}})_z$  significantly deviates from the reference, encouraging the robot to rise in place. The Penalty Action Rate Before Stand term ( $a_j - a_j^{\text{prev}}$ ) penalizes abrupt changes in joint actions during this phase, promoting smooth and gradual motions. Together, these rewards bias the policy toward physically stable, upright recovery while maintaining close adherence to the reference motion.

#### 4.4 Termination Conditions

Table 4: Bad Tracking Termination Conditions

Name	Expression
Reference Position Deviation	$\mathbb{I}_{\text{bad\_ref\_pos}}(k) = \mathbb{I}\left(\ \mathbf{p}_k^{\text{ref}} - \mathbf{p}_k^{\text{robot}}\ _2 > \tau_{\text{pos}}\right)$
Reference Orientation Deviation	$\mathbb{I}_{\text{bad\_ref\_ori}}(k) = \mathbb{I}\left( (\mathbf{R}_k^{\text{ref}})^{\top} \mathbf{g} - (\mathbf{R}_k^{\text{robot}})^{\top} \mathbf{g} _z > \tau_{\text{ori}}\right)$
Body Position Deviation	$\mathbb{I}_{\text{bad\_motion\_body\_pos}}(k) = \mathbb{I}\left(\exists b \in \mathcal{B} : \ \mathbf{p}_{k,b}^{\text{body,ref}} - \mathbf{p}_{k,b}^{\text{body,robot}}\ _2 > \tau_{\text{body}}\right)$

At each time step  $k$ , we define a bad tracking indicator as the logical disjunction of all failure conditions in Table 4:

$$\mathbb{I}_{\text{bad}}(k) = \mathbb{I}_{\text{bad\_ref\_pos}}(k) \vee \mathbb{I}_{\text{bad\_ref\_ori}}(k) \vee \mathbb{I}_{\text{bad\_motion\_body\_pos}}(k). \quad (19)$$

To avoid premature termination during recovering tasks, we accumulate the length of consecutive bad tracking steps:

$$L(k) = \begin{cases} L(k-1) + 1, & \text{if } \mathbb{I}_{\text{bad}}(k) = 1, \\ 0, & \text{otherwise.} \end{cases} \quad (20)$$

The termination condition is defined as

$$\mathbb{I}_{\text{bad\_tracking\_terminate}}(k) = \begin{cases} \mathbb{I}(L(k) \geq \tau_{\text{bad}}), & \text{if } \mathbb{I}_{\text{recovering}}(k) = 1, \\ \mathbb{I}_{\text{bad}}(k), & \text{otherwise,} \end{cases} \quad (21)$$

where  $\mathbb{I}_{\text{recovering}}(k)$  indicates a recovering task and  $\tau_{\text{bad}}$  denotes the maximum allowed length of consecutive bad tracking steps.

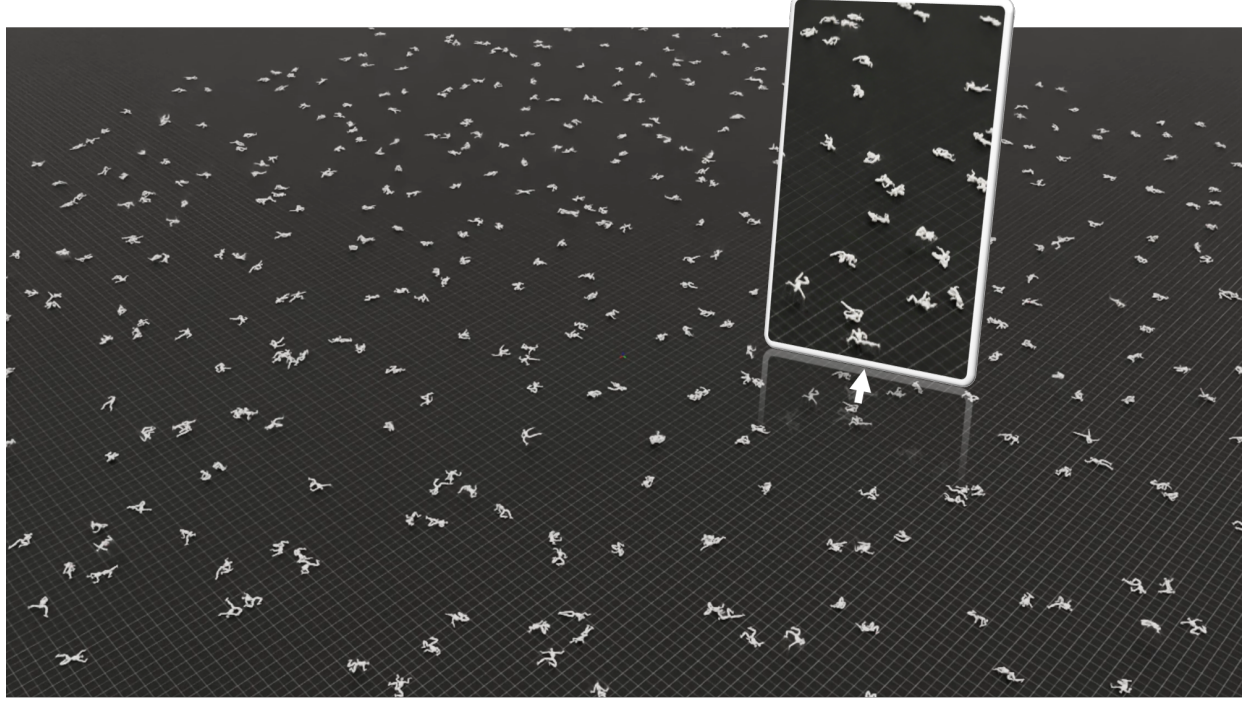


Figure 6: GRSI Visualization: Different fall postures resulting from dropping the robot from varying heights.

#### 4.5 Gravity-based Randomized State Initialization ( $\mathcal{D}_{\text{GRSI}}$ )

As illustrated in Fig. 6, to account for the high variability of post-fall configurations, we construct a diverse set of recovery initial states through physics-driven sampling. Specifically, the robot is initialized in a zero-torque mode and released under gravity with randomized contact friction, allowing the system dynamics to naturally generate a wide range of fallen configurations characterized by base position  $\mathbf{p}$ , base orientation  $\mathbf{r}$ , and joint configuration  $\theta$ . The resulting samples are collected to form the fall-recovery dataset  $\mathcal{D}_{\text{GRSI}}$ .

To further increase the coverage of the initial state distribution, we augment the dataset by randomly re-combining the rotational components  $(\mathbf{r}, \theta)$ , inducing different global orientation relationships while preserving local contact structures. This augmentation yields a diverse set of initial joint states  $\mathbf{q}_0$ , which improves the robustness and generalization of the learned recovery policy across a wide spectrum of fallen poses.

## 5 Experiments

In this section, we conduct a comprehensive evaluation of *KungFu Athletes* through both simulation and real-world experiments. Our experimental study is designed to answer the following questions:

- **Q1:** Does *KungFu Athletes* achieve better performance on highly dynamic motions compared to prior methods in simulation?
- **Q2:** Are the proposed reward designs effective in improving motion tracking performance?
- **Q3:** Can *KungFu Athletes* reliably recover from arbitrary initial postures?
- **Q4:** How does *KungFu Athletes* perform under real-world deployment?

### 5.1 Experimental Setup

We evaluate *KungFu Athletes* in both simulated and real-world environments. For training, we use Isaac Sim 5.0 as the simulation platform, while MuJoCo is employed for evaluation to reduce simulator bias. The training data is drawn from our proposed *KungFu Athletes* dataset, which contains highly dynamic, long-horizon, and balance-challenging

motions as described in Section 3.1. All training and evaluation are conducted on a single NVIDIA A100 GPU with 80GB memory.

For real-world experiments, we deploy the learned policy on the Unitree G1 humanoid robot, which has 29 degrees of freedom and a height of approximately 1.3 meters.

**Evaluation Metrics.** We evaluate motion tracking performance using the following metrics:

- **Success Rate (Succ., %):** A trial is considered failed if any joint position tracking error exceeds 0.5 m, the orientation error exceeds 0.8 rad, or the robot falls during execution.
- **Root-relative Mean Per-Body Orientation Error ( $E_{mpboe}$ ,  $10^{-2}$  rad):** Measures the average orientation tracking error for each body part.
- **Smoothness:** Measured by the average action rate between consecutive frames, where lower values indicate smoother motions.

**Training Details.** We adopt FastSAC [37] as the reinforcement learning algorithm. The actor network consists of three fully connected layers, while the critic comprises two networks with four layers each. Other hyperparameters follow the default settings in FastSAC.

For all recovery-related rewards, the tracking threshold on the shoulder height along the  $z$ -axis is set to 1.0. In the feet slip penalty, we consider foot slippage to occur when the contact force along the  $z$ -axis exceeds 8, under which lateral ( $x$ - $y$ ) foot velocity is penalized.



Figure 7: Under conditions free from external interference, we compared the performance of the BeyondMimic model (top sequence) with that of the model incorporating a fall recovery task (bottom sequence) during the single-leg standing task. Experimental results demonstrate that adding the fall recovery task significantly enhances BeyondMimic’s ability to handle falls and maintain balance.

**Domain Randomization.** Following the domain randomization protocol in FastSAC [37], we apply a comprehensive set of stochastic perturbations to improve robustness and sim-to-real generalization during locomotion training. Specifically, at setup time, we randomize physical and actuator properties, including link and base masses, ground friction, base center-of-mass offsets, actuator PD gains, and action delays, while optionally injecting torque disturbances and joint position biases. At reset, the robot state is further diversified by randomizing joint configurations, actuator states, push schedules, and control delays to prevent overfitting to specific initial conditions. During rollout, external pushes with randomized timing and magnitude are applied online to emulate unexpected disturbances. Together, these randomized factors cover uncertainties in dynamics, actuation, sensing, and external interactions, enabling the learned policy to remain stable under a wide range of environmental and model variations.

## 5.2 Motion Tracking Performance

**Ablation Study on Hybrid Rewards.** To answer **Q2**, we conduct an ablation study on the proposed hybrid reward design. We select the most challenging motion sequence in our dataset, consisting of 1307 frames and including multiple single-leg stances and punching motions. Each method is evaluated over six independent trials, and we report the average performance.

Table 5 and Figure 7 summarizes the experimental results. To ensure fairness, directional error and smoothness are computed only up to the point of failure. The baseline model, BeyondMimic, fails to maintain single-leg standing even

Table 5: Simulation performance comparison in the ablation study

Method	$E_{\text{mpboe}}$	Succ.	Smooth
BeyondMimic	12.55	0/6	14.2
w/ recover task	40.39	6/6	18.6
w/ recover task + feet slip (w=3)	25.27	6/6	19.2
w/ recover task + feet slip (w=5)	19.93	6/6	18.0

without perturbations, resulting in falls in all trials. After incorporating the fall-recovery task, the model no longer falls in the absence of perturbations and exhibits improved balance, indicating that the fall-recovery objective enhances the model’s understanding of balance maintenance.

The model trained with the recovery task (*w/ recover task*) achieves a significantly higher success rate, completing all trials without falling. Although this variant exhibits larger orientation errors and reduced smoothness compared to BeyondMimic, it demonstrates substantially improved robustness.

By further incorporating the feet slip penalty and adjusting its weight from 3 to 5, orientation tracking error is notably reduced. While a weight of 3 slightly degrades smoothness, increasing the weight to 5 improves both tracking accuracy and motion smoothness, even surpassing the recovery-only model.

Beyond quantitative metrics, we observe qualitative improvements in challenging motions such as cross-leg stepping. Without additional regularization, the recovery-enabled policy tends to adopt conservative behaviors, such as low foot lifting and ground scraping, to maintain stability. By introducing action rate penalties on key joints (e.g., knee and ankle) and combining them with the feet slip penalty, the robot learns to execute cleaner, single-lift stepping motions without foot dragging. Inspired by prior work [28], we further introduce a center-of-mass (CoM) alignment reward. Without this term, the CoM deviates from the support foot during single-l

## 6 Acknowledgement

The video materials used in this paper are primarily sourced from a series of publicly released martial arts training and competition demonstration videos by Xie Yuanhang. Xie Yuanhang is an athlete of the Guangxi Wushu Team, a National-Level Elite Athlete of China, and holds the rank of Chinese Wushu 6th Duan. He achieved third place in the Wushu Taolu event at the 10th National Games of the People’s Republic of China. His demonstrations cover Changquan, Nanquan, weapon routines, and Taijiquan (including Taijijian), and are of high professional and instructional value. We sincerely thank Xie Yuanhang for granting permission to use his publicly available videos for research and academic purposes only.

## References

- [1] Justin Carpentier, Rohan Budhiraja, and Nicolas Mansard. Learning feasibility constraints for multicontact locomotion of legged robots. In *Robotics: Science and Systems*, page 9p. Cambridge, MA, 2017.
- [2] Robin Deits, Scott Kuindersma, Matthew P Kelly, Twan Koolen, Yeuhi Abe, and Benjamin Stephens. Robot movement and online trajectory optimization, December 5 2023. US Patent 11,833,680.
- [3] Ilija Radosavovic, Tete Xiao, Bike Zhang, Trevor Darrell, Jitendra Malik, and Koushil Sreenath. Real-world humanoid locomotion with reinforcement learning. *Science Robotics*, 9(89):eadi9579, 2024.
- [4] Rajesh Subburaman, Nikos G Tsagarakis, and Jinh Lee. Online rolling motion generation for humanoid falls based on active energy control concepts. In *2018 IEEE-RAS 18th International Conference on Humanoid Robots (Humanoids)*, pages 1–7. IEEE, 2018.
- [5] Chuanyu Yang, Can Pu, Guiyang Xin, Jie Zhang, and Zhibin Li. Learning complex motor skills for legged robot fall recovery. *IEEE Robotics and Automation Letters*, 8(7):4307–4314, 2023.
- [6] Xue Bin Peng, Pieter Abbeel, Sergey Levine, and Michiel van de Panne. DeepMimic: Example-Guided Deep Reinforcement Learning of Physics-Based Character Skills. *ACM Transactions on Graphics*, 37(4):1–14, August 2018.
- [7] Zipeng Fu, Qingqing Zhao, Qi Wu, Gordon Wetzstein, and Chelsea Finn. HumanPlus: Humanoid Shadowing and Imitation from Humans, June 2024.



Figure 8: Recovery from falls in various lying positions.

- [8] Kangning Yin, Weishuai Zeng, Ke Fan, Minyue Dai, Zirui Wang, Qiang Zhang, Zheng Tian, Jingbo Wang, Jiangmiao Pang, and Weinan Zhang. UniTracker: Learning Universal Whole-Body Motion Tracker for Humanoid Robots, September 2025.
- [9] Weishuai Zeng, Shunlin Lu, Kangning Yin, Xiaojie Niu, Minyue Dai, Jingbo Wang, and Jiangmiao Pang. Behavior Foundation Model for Humanoid Robots, September 2025.
- [10] Naureen Mahmood, Nima Ghorbani, Nikolaus F. Troje, Gerard Pons-Moll, and Michael J. Black. AMASS: Archive of Motion Capture as Surface Shapes, April 2019.
- [11] Zixuan Chen, Mazeyu Ji, Xuxin Cheng, Xuanbin Peng, Xue Bin Peng, and Xiaolong Wang. Gmt: General motion tracking for humanoid whole-body control. *arXiv preprint arXiv:2506.14770*, 2025.
- [12] Yanjie Ze, Zixuan Chen, João Pedro Araújo, Zi ang Cao, Xue Bin Peng, Jiajun Wu, and C. Karen Liu. Twist: Teleoperated whole-body imitation system. *arXiv preprint arXiv:2505.02833*, 2025.
- [13] Félix G. Harvey, Mike Yurick, Derek Nowrouzezahrai, and Christopher Pal. Robust motion in-betweening. 39(4), 2020.
- [14] Tao Huang, Huayi Wang, Junli Ren, Kangning Yin, Zirui Wang, Xiao Chen, Feiyu Jia, Wentao Zhang, Junfeng Long, Jingbo Wang, and Jiangmiao Pang. Towards Adaptable Humanoid Control via Adaptive Motion Tracking, October 2025.
- [15] Qiayuan Liao, Takara E. Truong, Xiaoyu Huang, Yuman Gao, Guy Tevet, Koushil Sreenath, and C. Karen Liu. BeyondMimic: From Motion Tracking to Versatile Humanoid Control via Guided Diffusion, November 2025.

[16] Sichen Li, Gang Wang, Yiming Pang, Panju Bai, Shihao Hu, Zhaojin Liu, Liquan Wang, and Jiawei Li. Learning agility and adaptive legged locomotion via curricular hindsight reinforcement learning. *Scientific Reports*, 14(1):28089, 2024.

[17] Zhengjie Xu, Ye Li, Kwan-yee Lin, and Stella X Yu. Unified humanoid fall-safety policy from a few demonstrations. *arXiv preprint arXiv:2511.07407*, 2025.

[18] Yitang Li, Zhengyi Luo, Tonghe Zhang, Cunxi Dai, Anssi Kanervisto, Andrea Tirinzoni, Haoyang Weng, Kris Kitani, Mateusz Guzek, Ahmed Touati, et al. Bfm-zero: A promptable behavioral foundation model for humanoid control using unsupervised reinforcement learning. *arXiv preprint arXiv:2511.04131*, 2025.

[19] Ziyu Meng, Tengyu Liu, Le Ma, Yingying Wu, Ran Song, Wei Zhang, and Siyuan Huang. Safefall: Learning protective control for humanoid robots. *arXiv preprint arXiv:2511.18509*, 2025.

[20] Zhengjie Xu, Ye Li, Kwan-yee Lin, and Stella X. Yu. Unified Humanoid Fall-Safety Policy from a Few Demonstrations, November 2025.

[21] Qingwei Ben, Feiyu Jia, Jia Zeng, Junting Dong, Dahua Lin, and Jiangmiao Pang. Homie: Humanoid locomanipulation with isomorphic exoskeleton cockpit. *arXiv preprint arXiv:2502.13013*, 2025.

[22] Rui Zhong, Yizhe Sun, Junjie Wen, Jinming Li, Chuang Cheng, Wei Dai, Zhiwen Zeng, Huimin Lu, Yichen Zhu, and Yi Xu. Humanoidexo: Scalable whole-body humanoid manipulation via wearable exoskeleton. *arXiv preprint arXiv:2510.03022*, 2025.

[23] Yanjie Ze, Siheng Zhao, Weizhuo Wang, Angjoo Kanazawa, Rocky Duan, Pieter Abbeel, Guanya Shi, Jiajun Wu, and C Karen Liu. Twist2: Scalable, portable, and holistic humanoid data collection system. *arXiv preprint arXiv:2511.02832*, 2025.

[24] Zhengyi Luo, Ye Yuan, Tingwu Wang, Chenran Li, Sirui Chen, Fernando Castañeda, Zi-Ang Cao, Jiefeng Li, David Minor, Qingwei Ben, et al. Sonic: Supersizing motion tracking for natural humanoid whole-body control. *arXiv preprint arXiv:2511.07820*, 2025.

[25] Zehong Shen, Huaijin Pi, Yan Xia, Zhi Cen, Sida Peng, Zechen Hu, Hujun Bao, Ruizhen Hu, and Xiaowei Zhou. World-Grounded Human Motion Recovery via Gravity-View Coordinates. In *SIGGRAPH Asia 2024 Conference Papers*, pages 1–11, December 2024.

[26] Tairan He, Jiawei Gao, Wenli Xiao, Yuanhang Zhang, Zi Wang, Jiashun Wang, Zhengyi Luo, Guanqi He, Nikhil Sobanbab, Chaoyi Pan, Zeji Yi, Guannan Qu, Kris Kitani, Jessica Hodgins, Linxi "Jim" Fan, Yuke Zhu, Changliu Liu, and Guanya Shi. ASAP: Aligning Simulation and Real-World Physics for Learning Agile Humanoid Whole-Body Skills, April 2025.

[27] Weiji Xie, Jinrui Han, Jiakun Zheng, Huanyu Li, Xinzhe Liu, Jiyuan Shi, Weinan Zhang, Chenjia Bai, and Xuelong Li. Kungfubot: Physics-based humanoid whole-body control for learning highly-dynamic skills. *arXiv preprint arXiv:2506.12851*, 2025.

[28] Tong Zhang, Boyuan Zheng, Ruiqian Nai, Yingdong Hu, Yen-Jen Wang, Geng Chen, Fanqi Lin, Jiongye Li, Chuye Hong, Koushil Sreenath, and Yang Gao. HuB: Learning Extreme Humanoid Balance, August 2025.

[29] Yixuan Pan, Ruoyi Qiao, Li Chen, Kashyap Chitta, Liang Pan, Haoguang Mai, Qingwen Bu, Hao Zhao, Cunyuan Zheng, Ping Luo, and Hongyang Li. Agility Meets Stability: Versatile Humanoid Control with Heterogeneous Data, November 2025.

[30] Mazeyu Ji, Xuanbin Peng, Fangchen Liu, Jialong Li, Ge Yang, Xuxin Cheng, and Xiaolong Wang. ExBody2: Advanced Expressive Humanoid Whole-Body Control, March 2025.

[31] Zhenguo Sun, Yibo Peng, Yuan Meng, Xukun Li, Bo-Sheng Huang, Zhenshan Bing, Xinlong Wang, and Alois Knoll. RobotDancing: Residual-Action Reinforcement Learning Enables Robust Long-Horizon Humanoid Motion Tracking, September 2025.

[32] Xialin He, Runpei Dong, Zixuan Chen, and Saurabh Gupta. Learning getting-up policies for real-world humanoid robots. *arXiv preprint arXiv:2502.12152*, 2025.

[33] Tao Huang, Junli Ren, Huayi Wang, Zirui Wang, Qingwei Ben, Muning Wen, Xiao Chen, Jianan Li, and Jiangmiao Pang. Learning humanoid standing-up control across diverse postures. *arXiv preprint arXiv:2502.08378*, 2025.

[34] Jonathan Spraggett. Learning to get up across morphologies: Zero-shot recovery with a unified humanoid policy. *arXiv preprint arXiv:2512.12230*, 2025.

[35] Abraham Savitzky and Marcel JE Golay. Smoothing and differentiation of data by simplified least squares procedures. *Analytical chemistry*, 36(8):1627–1639, 1964.

[36] Younggyo Seo, Carmelo Sferrazza, Haoran Geng, Michal Nauman, Zhao-Heng Yin, and Pieter Abbeel. Fasttd3: Simple, fast, and capable reinforcement learning for humanoid control. *arXiv preprint arXiv:2505.22642*, 2025.

- [37] Younggyo Seo, Carmelo Sferrazza, Juyue Chen, Guanya Shi, Rocky Duan, and Pieter Abbeel. Learning Sim-to-Real Humanoid Locomotion in 15 Minutes, December 2025.
- [38] Yanjie Ze, Zixuan Chen, João Pedro Araújo, Zi-ang Cao, Xue Bin Peng, Jiajun Wu, and C. Karen Liu. TWIST: Teleoperated Whole-Body Imitation System, May 2025.